PROCEEDINGS A

rspa.royalsocietypublishing.org

Research

Cite this article: Ali SZ, Dey S. 2017 Origin of the scaling laws of sediment transport. *Proc. R. Soc. A* **473**: 20160785.
http://dx.doi.org/10.1098/rspa.2016.0785

Received: 19 October 2016
Accepted: 15 December 2016

Subject Areas:
fluid mechanics

Keywords:
turbulent flow, fluid–particle interaction, sediment transport

Author for correspondence:
Subhasish Dey
e-mail: sdey@iitkgp.ac.in

Downloaded from https://royalsocietypublishing.org/ on 25 October 2022

Origin of the scaling laws of sediment transport

Sk Zeeshan Ali and Subhasish Dey

Department of Civil Engineering, Indian Institute of Technology Kharagpur, West Bengal, India

SD, 0000-0002-1952-4491

In this paper, we discover the origin of the scaling laws of sediment transport under turbulent flow over a sediment bed, for the first time, from the perspective of the phenomenological theory of turbulence. The results reveal that for the incipient motion of sediment particles, the densimetric Froude number obeys the '$(1+\sigma)/4$' scaling law with the relative roughness (ratio of particle diameter to approach flow depth), where σ is the spectral exponent of turbulent energy spectrum. However, for the bedforms, the densimetric Froude number obeys a '$(1+\sigma)/6$' scaling law with the relative roughness in the enstrophy inertial range and the energy inertial range. For the bedload flux, the bedload transport intensity obeys the '3/2' and '$(1+\sigma)/4$' scaling laws with the transport stage parameter and the relative roughness, respectively. For the suspended load flux, the non-dimensional suspended sediment concentration obeys the '$-\mathcal{Z}$' scaling law with the non-dimensional vertical distance within the wall shear layer, where $\mathcal{Z}$ is the Rouse number. For the scour in contracted streams, the non-dimensional scour depth obeys the '$4/(3-\sigma)$', '$-4/(3-\sigma)$' and '$-(1+\sigma)/(3-\sigma)$' scaling laws with the densimetric Froude number, the channel contraction ratio (ratio of contracted channel width to approach channel width) and the relative roughness, respectively.

1. Introduction

The genesis of the *phenomenological theory* of turbulence was due to Kolmogorov [1], who derived the scaling laws of the fully developed steady-state turbulence originating from the unverified but conceivable tenets [2]. The phenomenological theory, however, provides an easy means (preserving the scientific basis) predicting the scaling laws of several fluid flow phenomena governed by the turbulence. The primary advantage of the applications of this theory in analysing the classical

THE ROYAL SOCIETY PUBLISHING

© 2017 The Author(s) Published by the Royal Society. All rights reserved.

Downloaded from https://royalsocietypublishing.org/ on 25 October 2022

problems on fluid mechanics is that it allows us to obtain the desired results in a much simpler way requiring less heuristic arguments. In particular, such theory establishes a unique relationship between the dependent variable and the independent variables of a problem by means of the turbulence scaling laws, in which the independent variables contain single free exponents. But this is not the case for an empirical or semi-empirical law describing a problem on fluid mechanics. The empirical or semi-empirical laws mostly originate from the dimensional analysis with systematic arguments, containing numerous free exponents, which are determined from the regression analyses using the experimental and/or field data. Therefore, empirical or semi-empirical laws proposed by different investigators for a specific problem on fluid mechanics may render different results. By contrast, the phenomenological theory of turbulence provides a simple but logical treatment with a scientific background to obtain a unique relationship between the dependent variable and the independent variables by controlling the degrees of freedom of the exponents. However, such a relationship includes a multiplicative constant, which should be obtained via experiments.

Over decades, the applications of the phenomenological theory of turbulence have received much attention by scientists and engineers, particularly in modelling turbulent flows [2,3]. Some applications of the phenomenology of turbulence include (i) counting the degrees of freedom, (ii) comparing the microscopic and the macroscopic length scales, and (iii) obtaining the probability distribution function of velocity gradients and the law of the energy decay [2]. Nikora [4] derived the origin of the '−1' spectral law in a wall-bounded turbulent flow by applying the phenomenology of turbulence. The phenomenology of turbulence was also applied to obtain the scaling and the similarity laws in open-channel flows [5].

Here, an attempt is made, for the first time, to explore the origin of the scaling laws of sediment transport from the phenomenological theory of turbulence. We apply the momentum transfer theory in conjunction with the laws of turbulent energy spectrum to find the link between the laws of sediment transport and the turbulent energy spectrum.

The paper is organized as follows. In §2, a brief description of the laws of turbulent energy spectrum is presented. The scaling law of threshold velocity is explained in §3. In §4, the scaling law of bedload flux is obtained. The scaling law of suspended load flux is deduced in §5, while the scaling law of scour in a contracted stream is derived in §6. Finally, conclusion is drawn in §7.

2. Laws of turbulent energy spectrum

The characteristic velocity v_l of a turbulent eddy, having a characteristic length l, is expressed as

$$v_l \sim \left(\int_{l^{-1}}^{\infty} E(k)\, \mathrm{d}k \right)^{1/2}, \tag{2.1}$$

where $E(k)$ is the energy spectrum function, k is the wavenumber and the symbol '$\sim$' represents the 'scales with'. If the $E(k)$ is characterized by the spectral exponent σ, from dimensional analysis, it can be written $E(k) \sim V_L^2 L^{1+\sigma} k^{\sigma}$, where V_L is the velocity scale associated with the integral length scale L representing the energy containing turbulent eddies. Substituting this form of $E(k)$ into equation (2.1) yields

$$v_l \sim V_L \left(\frac{l}{L} \right)^{-(1+\sigma)/2}. \tag{2.2}$$

The above relationship simply relates the microscopic and macroscopic scales of the turbulent flow aided by the spectral exponent. It is well known that when the large scale (that is, the integral length scale or the forcing scale) and the small scale (that is, the dissipation scale) are separated in the E–k plane, it yields two inertial ranges: the energy inertial range and the enstrophy (half of square of vorticity) inertial range [6]. From the fundamental tenet of two-dimensional turbulence, there exist two plausible cascades (figure 1): (i) the energy inverse cascade and (ii) the enstrophy cascade. In the energy inverse cascade, energy flows in the reverse direction (that is from small to large scales), while in the enstrophy cascade, the enstrophy

Downloaded from https://royalsocietypublishing.org/ on 25 October 2022

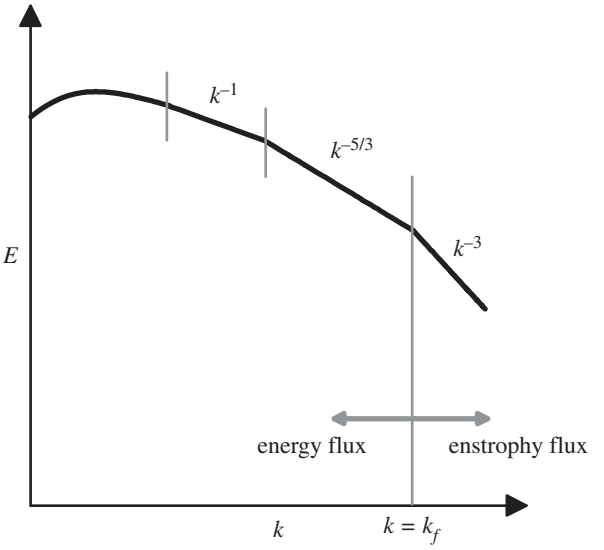

Figure 1. Schematic of turbulent energy spectrum illustrating the spectral laws.

flows in the forward direction (that is from large to small scales). Unlike three-dimensional turbulence, two-dimensional turbulence is not characterized by the vortex stretching. From the assumption of spectral localness of the cascades, the energy spectrum function $E(k)$ in the energy inertial range or in the enstrophy inertial range at a given wavenumber k, depends solely on k and local straining rate. Therefore, the energy inverse cascade yields the '$-5/3$' spectral law: $E(k) \sim \varepsilon^{2/3}k^{-5/3}$, where ε is the turbulent kinetic energy (TKE) dissipation rate. In contrast, the enstrophy cascade yields the '-3' spectral law: $E(k) \sim \beta^{2/3}k^{-3}$, where β is the enstrophy dissipation rate. Assuming that the energy flux is being fed in to a band of wavenumbers (approx. k_f), known as the forcing wavenumber, the '$-5/3$' spectral law persists for $k \ll k_f$ for a sufficiently large Reynolds number, while the '-3' spectral law persists for $k \gg k_f$ up to the dissipation range, where molecular viscosity prevails (figure 1). Another well-known spectral law in the wall-bounded turbulent flow is the '-1' spectral law of the energy spectrum (figure 1): $E(k) \sim u_*^2 k^{-1}$ for $L^{-1} \leq k \leq z^{-1}$ [4], where u_* is the shear velocity and z is the vertical distance. Importantly, for two-dimensional turbulence, the energy transfers from small to large scales in the energy inverse cascade preserving the '$-5/3$' spectral law. In contrast, if the energy transfers otherwise (as in case of three-dimensional turbulence), then the '$-5/3$' spectral law would not make any difference in the spectral exponent [7]. Therefore, irrespective of the direction of energy transfer, the '$-5/3$' spectral law in the energy inertial range is valid for both two- and three-dimensional turbulence (figure 1). Specifically, the two-dimensional turbulence is an idealized case, because the natural flows over a sediment bed can withstand two-dimensionality only for a limited range of scales.

The momentum transfer theory based on the turbulent energy spectrum revealed the features of two-dimensional turbulence by linking the friction factor with the Reynolds number and the roughness height [8]. However, the scaling law of the friction factor for two-dimensional turbulence in the energy inertial range remains the same for the three-dimensional turbulence. This is because for both two- and three-dimensional turbulence, the energy spectrum function obeys the '$-5/3$' spectral law in the energy inertial range. Rutgers [7] reported that in two-dimensional turbulence, the energy inverse cascade and the enstrophy cascade can occur simultaneously or separately depending on how the energy is being fed into the system (uniform energy injection or oscillating energy injection into the flow). Here, we attempt to find the origin of the scaling laws of sediment transport by means of laws of turbulent energy spectrum. We

Downloaded from https://royalsocietypublishing.org/ on 25 October 2022

consider four classical sediment transport problems, which involve the interaction between the turbulent flow and the sediment particles. These problems include the determination of the scaling laws of threshold velocity, bedload flux, suspended load flux and scour in a contracted stream. Such classical problems are the fundamental aspects in sediment transport research; and therefore, this study intends to analyse such problems to provide an insight of the underlying flow physics.

3. The scaling law of threshold velocity

(a) Theoretical analysis

Let us consider a fully developed turbulent stream flowing over a sediment bed as sketched in figure 2. The mean flow depth is h, the mean flow velocity is U and the bed roughness height is k_s. As the k_s can be scaled with the nominal diameter d of the sediment particle, we can write $k_s \sim d$ [9]. Here, the nominal diameter refers to the diameter of a sphere having the same volume as that of a given sediment particle. A competent velocity, commonly known as *threshold velocity*, is defined as the near-bed velocity u_c or the mean flow velocity U_c that is marginally sufficient to initiate the particle motion at the surface of a sediment bed. This phenomenon is known as the *incipient motion* of sediment particles [10,11]. The use of the near-bed flow velocity to quantify the inception of sediment particles remains elusive owing to numerous complications involved in the velocity measurements at the particle level. On the other hand, the concept of mean flow velocity to determine the threshold criterion is rather consistent since the mean flow velocity for a given flow discharge is easy to determine. To estimate the near-bed flow velocity or the mean flow velocity, the assumption of time-averaged longitudinal flow velocity is an essential prerequisite. Since an accurate estimation of the near-bed flow velocity is a difficult proposition, the time-averaged velocity distribution is often extrapolated up to the particle level to obtain a crude estimation of the near-bed flow velocity as illustrated in figure 2. Therefore, in this study, we consider the mean flow velocity U_c to represent the threshold velocity. Several investigators experimentally found the threshold velocity of sediment particles under different flow regimes [12–18]. Various empirical formulae to predict the threshold velocity were also reported in the literature. An extensive survey of these formulae was done by García [9] and Dey [19]. The empirical formulae reveal that for the hydraulically rough flow regime, the threshold velocity in non-dimensional form can be expressed as a functional relationship as follows:

$$\mathcal{F}_{dc} = \frac{U_c}{(\Delta g d)^{1/2}} = K f(\zeta), \tag{3.1}$$

where $\mathcal{F}_d$ is the densimetric Froude number, Δ is the submerged relative density of sediment particles [$=(\rho_p - \rho_f)/\rho_f$], ρ_p is the mass density of sediment particle, ρ_f is the mass density of fluid, K is the multiplicative constant and ζ is the relative roughness ($=d/h$). Subscript 'c' denotes the threshold value.

The Shields parameter Θ ($=\tau_0/(\Delta\rho_f g d)$, where τ_0 is the bed shear stress and g is the gravitational acceleration) is commonly used to define the sediment threshold condition in hydraulically smooth and transitional regimes, while it has a constant value (=0.56) in hydraulically rough flow regime [19]. However, the Shields parameter Θ and the densimetric Froude number $\mathcal{F}_d$ can be linked as $\Theta = g(\mathcal{F}_d/C_R)^2$, where C_R is the Chézy coefficient. This relationship is also valid under threshold condition and reveals that for a fixed value of Θ, the $\mathcal{F}_d$ is proportional to the C_R. Moreover, in the hydraulically rough flow regime, the C_R depends on the relative roughness ζ either logarithmically or by a power of '1/6' [19]. Therefore, at threshold condition, it yields $\mathcal{F}_{dc} \sim \zeta^{-1/6}$, which is in conformity with equation (3.1). Here, we show that the same scaling law can be derived by applying the spectral law in the energy inertial range in conjunction with the momentum transfer theory of turbulent eddies. In this study, we explore that the '−1/6' scaling law is legitimate within the energy inertial range, but beyond this range, different scaling laws are valid according to the laws of turbulent energy spectrum.

Downloaded from https://royalsocietypublishing.org/ on 25 October 2022

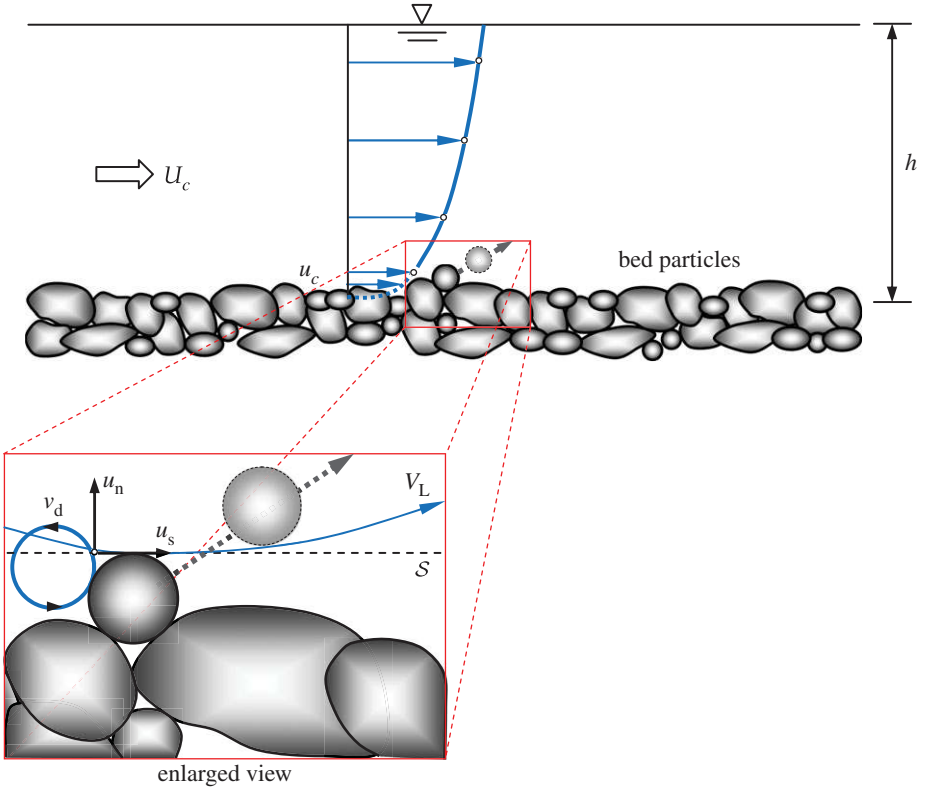

Figure 2. Schematic of turbulent flow over a loose sediment bed. The mean flow depth is h, the mean flow velocity is U and the velocity at the particle level is u. Subscript 'c' denotes the threshold condition for the motion of sediment particles. Enlarged view of the bed particles shows a typical interaction between the target particle and the localized turbulent eddy in the immediate vicinity of the bed surface. The horizontal dashed line represents the wetted surface $\mathcal{S}$ tangential to the summit of the target particle at the threshold of dislodgment. The velocity scale of the largest eddy is represented by V_L, while the velocity scale of the localized eddy is denoted by v_d. The fluctuations of tangential and normal velocity components are u_s and u_n, respectively. (Online version in colour.)

We now intend to understand as to what extent the formulation (3.1) can be obtained from the dimensional analysis. Let us consider seven plausible variables: U_c, h, d, ρ_p, ρ_f, g and ν, where ν is the coefficient of kinematic viscosity. Thus, in functional form, the equation $f(U_c, h, d, \Delta g, \rho_f, \nu) = 0$ exists. By dimensional analysis, we obtain the following functional relationship:

$$\mathcal{F}_{dc} = \phi(\zeta, D_*), \tag{3.2}$$

where D_* is the particle parameter $[=(d\Delta g/\nu^2)^{1/3}]$. Comparing equations (3.1) and (3.2), it is revealed that the dimensional analysis produces the similar functional form as that obtained from empirical formulae, with the exception that the D_* is an independent variable in equation (3.2). Notwithstanding that the relationship (3.1) is valid for the hydraulically rough flow regime, where the $\mathcal{F}_{dc}$ is invariant of D_*. Now, we attempt to explore the origin of the scaling law of equation (3.2) from the perspective of the turbulent energy spectrum.

Theorem 3.1. *For the incipient motion of sediment particles, the densimetric Froude number obeys the '$(1+\sigma)/4$' scaling law with the relative roughness.*

Proof. Let us consider the length scale $l \in (\eta, L)$ in the energy inertial range, where η is the Kolmogorov dissipation length scale. If t_l is the eddy turnover time that corresponds to l, then $t_l \sim l/v_l$. Therefore, the energy flux E_l is $E_l \sim v_l^2/t_l \sim v_l^3/l$. In the energy inertial range, the TKE

Downloaded from https://royalsocietypublishing.org/ on 25 October 2022

production rate and the TKE dissipation rate maintain energy equilibrium by balancing each other. It therefore implies that the E_l equals the mean TKE dissipation rate ε. Hence, we obtain $E_l = \varepsilon \sim v_l^3/l$ [20]. However, for $l \sim L$, we can write $\varepsilon \sim V_L^3/L$. Thus, the above consideration implies $v_l \sim V_L(l/L)^{1/3}$. Importantly, the same relationship can be obtained if $\sigma = -5/3$ is substituted in equation (2.2). The L and V_L can be easily scaled with the flow depth h and the mean flow velocity U, respectively, yielding $v_l \sim U(l/h)^{1/3}$.

It is pertinent to mention that the Kolmogorov's scaling laws are valid for a highly idealized turbulence case, particularly if the small-scale motions are homogeneous and isotropic. In practical situations, turbulent flow in the vicinity of the sediment beds shows a considerable departure from the idealized framework because of the substantial modification of the mean flow field due to the bed roughness heterogeneity and fluctuation anisotropy [21]. However, the literature survey reveals that the Kolmogorov's scaling laws are also applicable for non-homogeneous and anisotropic flows [22]. We, therefore, conclude that the applicability of the phenomenology of turbulence to describe the small-scale motions for the sediment transport problems is no longer ambiguous.

Let us now focus on the fluid–sediment interaction in the immediate vicinity of the sediment bed as depicted in figure 2 (see the enlarged view). Here, a localized turbulent eddy interacting with the target particle plays a major role to dislodge the particle from its stabilized position. Let us seek the scaling law of the Reynolds shear stress τ_t developed due to the localized eddy at an imaginary wetted surface $\mathcal{S}$ tangential to the summit of the target particle forming the imaginary surface of the sediment bed. The Reynolds shear stress τ_t is expressed as $\tau_t = \rho_f \overline{u_s u_n}$ [23], where u_s and u_n are the velocity fluctuations tangential and normal to the $\mathcal{S}$, respectively. The overbar denotes the time-averaging of a quantity. In fact, the τ_t is triggered by the momentum transfer across the imaginary wetted surface $\mathcal{S}$. Above the surface $\mathcal{S}$, the flow velocity scales with V_L or U. As a result, the fluid transmits a substantial horizontal component of momentum per unit volume ($\sim \rho_f U$) tangential to the $\mathcal{S}$. On the other hand, below the $\mathcal{S}$, the flow velocity is significantly small. Thus, the fluid transmits an insignificant horizontal component of momentum per unit volume tangential to the $\mathcal{S}$. The localized eddy, bestriding the wetted surface $\mathcal{S}$, transfers the fluid of high and low momentum fluxes tangential to the $\mathcal{S}$ in the downward and the upward directions, respectively, across the $\mathcal{S}$. Thus, the net transfer of momentum flux across the $\mathcal{S}$ is accomplished by the velocity normal to the $\mathcal{S}$ induced by the localized eddy. Therefore, the Reynolds shear stress developed at the $\mathcal{S}$ due to the momentum transfer yields $\tau_t \sim \rho_f U u_n$. To envisage the dominant eddy bestriding the $\mathcal{S}$, we note that the eddies of size greater than l ($l \sim k_s$ or $l \sim d$) feebly contribute to the velocity normal to the $\mathcal{S}$. By contrast, the eddies of sizes smaller than l perfectly adjust within the inter particles space providing a significant contribution to the velocity normal to the $\mathcal{S}$. Hence, the eddies of sizes l ($l \sim k_s$ or $l \sim d$) contribute their characteristic velocity v_l normal to the $\mathcal{S}$. Thus, we can conceptually write $u_n \sim v_{k_s} \sim v_d$ [8]. From equation (2.2), it follows:

$$v_{k_s} (\sim v_d) \sim U\left(\frac{k_s}{h}\right)^{-(1+\sigma)/2} \sim U\left(\frac{d}{h}\right)^{-(1+\sigma)/2} \sim U\zeta^{-(1+\sigma)/2}. \tag{3.3}$$

Thus, the τ_t is

$$\tau_t \sim \rho_f U v_d \sim \rho_f U^2 \zeta^{-(1+\sigma)/2}. \tag{3.4}$$

The threshold velocity U_c can be obtained by equating the Reynolds shear stress developed at the wetted surface $\mathcal{S}$ and the threshold bed shear stress τ_{0c}. The τ_{0c} can be related to the gravitational stress τ_g as $\tau_{0c} \sim \tau_g = (\rho_p - \rho_f) g d \Theta_c$, where Θ_c is the threshold Shields parameter being a function of the particle parameter D_*. Let us say $\Theta_c = G(D_*)$. Therefore, at an incipient motion of sediment particles, we can write $\tau_t \sim \tau_g$, which results in

$$\rho_f U_c^2 \zeta^{-(1+\sigma)/2} \sim (\rho_p - \rho_f) g d G(D_*) \Rightarrow \mathcal{F}_{dc} \sim \zeta^{(1+\sigma)/4} G^{1/2}(D_*). \tag{3.5}$$

Downloaded from https://royalsocietypublishing.org/ on 25 October 2022

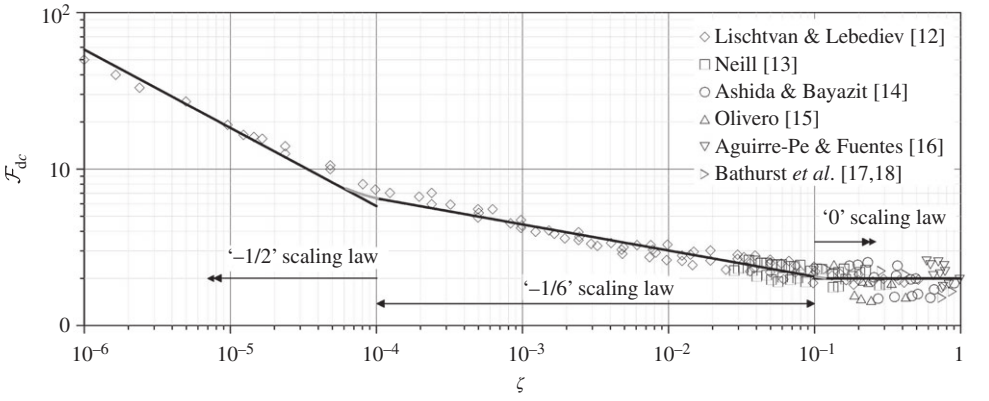

Figure 3. The threshold densimetric Froude number $\mathcal{F}_{dc}$ as a function of relative roughness ζ obeying the '−1/2', '−1/6' and '0' scaling laws, and the experimental data in earlier studies [12–18].

Note that for a hydraulically rough flow regime, the function $G(D_*)$ attains a constant value, as the Θ_c for rough flow is independent of D_*. ■

(b) Results and discussion

In the energy inertial range, we have $\sigma = -5/3$ yielding $\mathcal{F}_{dc} \sim \zeta^{-1/6}$. This relationship reveals that at an incipient motion of sediment particles, the densimetric Froude number obeys the '−1/6' scaling law with the relative roughness for a fully developed rough-turbulent flow. This scaling law is in conformity with the friction factor conjecture (Manning–Strickler relationship) as already derived before. Thus, we can conclude that the origin of the '−1/6' scaling law of the threshold densimetric Froude number with the relative roughness can be explained from the law of turbulent energy spectrum in the energy inertial range.

Importantly, the '−1/6' scaling law is legitimate when the characteristic particle diameter scales with the size of eddies in the energy inertial range. This condition allows us to restrict the '−1/6' scaling law within the limits: $5\eta \ll d \ll h$, where 5η represents the extent of viscous sublayer thickness. Substituting $\eta = \nu^{3/4}\varepsilon^{-1/4}$ and $\varepsilon \sim U^3/h$, the range of validity of the '−1/6' scaling law becomes

$$14.14\mathcal{R}^{-3/4} \ll \zeta \ll 1, \tag{3.6}$$

where $\mathcal{R}$ is the Reynolds number ($=4Uh/\nu$).

Figure 3 depicts the complete picture of the dependency of threshold densimetric Froude number $\mathcal{F}_{dc}$ on the ζ over a broad spectrum of ζ and the experimental data of several investigators [12–18]. A significant agreement between the '−1/6' scaling law and the experimental data is discernible over a wide range of ζ. From figure 3, it is evident that the range of validity of the '−1/6' scaling law, as shown in equation (3.6), can be replaced by the following range: $10^{-4} < \zeta < 10^{-1}$.

A close observation of figure 3 reveals that the experimental data lying in the range $10^{-4} < \zeta < 4 \times 10^{-4}$ slightly depart from the '−1/6' scaling law. The possible reason is attributed to the fact that for $\zeta < 4 \times 10^{-4}$, the characteristic particle diameter becomes close to the viscous sublayer thickness ($d \geq 5\eta$) and the flow becomes transitional smooth. For $\zeta < 10^{-4}$, the characteristic particle diameter essentially becomes of the order of the viscous sublayer thickness ($d \sim 5\eta$), and as a result of which the sediment particles are subjected to a smooth flow regime. Thus, the sediment particles are completely sheltered by the viscous sublayer and the momentum transfer becomes truly viscous. Therefore, the applicability of the '−1/6' scaling law does not hold. For such a scenario, the enstrophy cascade becomes dominant due to the smooth velocity field (two-dimensional turbulence); and the turbulent energy spectrum obeys the '−3' spectral

Downloaded from https://royalsocietypublishing.org/ on 25 October 2022

law (figure 1). Therefore, substituting $\sigma = -3$ in equation (3.5), we obtain $\mathcal{F}_{dc} \sim \zeta^{-1/2} G(D_*)$, suggesting a '$-1/2$' scaling law of the threshold densimetric Froude number with the relative roughness. It is evident that the experimental data respect the '$-1/2$' scaling law over a wide range of ζ ($10^{-6} < \zeta < 10^{-4}$). The '$-1/2$' scaling law indicates that for a given ζ, the threshold velocity required to dislodge the sediment particles is higher than that obtained from the '$-1/6$' scaling law. This is physically meaningful since the viscous sublayer acts as a barrier to protect the sediment particles (being of the order of viscous sublayer thickness) from the erosive action of flow resulting from the energetics of turbulent eddies in the energy inertial range. Thus, it indicates the requirement of a much higher velocity to dislodge the sediment particles in a hydraulically smooth flow regime. However, for $\zeta \ll 10^{-6}$, the resulting eddies belong to the dissipation range in the energy spectrum (of the order of the Kolmogorov's length scale) until they completely transfer the kinetic energy into heat.

On the other hand, when the relative roughness ζ becomes large ($\zeta \geq 10^{-1}$), the flow is characterized by the macro-turbulence resulting from the large eddies that belong to the energy containing range. As a result, the turbulent energy spectrum obeys the '-1' scaling law due to the presence of energy containing eddies. Thus, substituting $\sigma = -1$ in equation (3.5) yields $\mathcal{F}_{dc} \sim \zeta^0 G(D_*)$, suggesting a '0' scaling law of the threshold densimetric Froude number with the relative roughness. The '0' scaling law indicates that the threshold velocity is independent of the relative roughness. However, it is relevant to point out that the '0' scaling law holds when the '-1' spectral law is not disturbed by the large scale motions. A satisfactory agreement of the '0' scaling law with the experimental data trend is evident for $\zeta \geq 10^{-1}$ (figure 3). Importantly, when $\zeta \approx 1$, the proposed momentum transfer theory at the particle–fluid interface does not hold since the resulting eddies are unable to bestride the wetted surface. Therefore, the '0' scaling law is legitimate for $10^{-1} < \zeta \ll 1$ from the perspective of momentum transfer, although figure 3 reveals that the '0' scaling law still agrees well with the experimental data up to $\zeta \approx 1$.

The transition zones between the '$-1/2$' and '$-1/6$' scaling laws and the '$-1/6$' and '0' scaling laws are further depicted by faded solid lines in order to capture the behavioural features of the turbulent energy spectrum in the transition zones. Thus, figure 3 reveals the missing link between the threshold velocity law (densimetric Froude number as a function of relative roughness) and the laws of turbulent energy spectrum. Moreover, figure 3 can be linked with the Shields diagram for different flow regimes (hydraulically smooth, transitional and rough), depending on the values of $G(D_*)$. To be explicit, for a lower value of ζ, although the $G(D_*)$ does not attain a constant value, the laws of the spectrum are still valid because a multiplicative factor $G(D_*)$ can be applied to balance the momentum transfer (see equation (3.5)).

In the case of bedforms, the effective resistance to flow can be split into two parts: (i) the resistance due to forces experienced by individual particles, known as resistance due to particles or skin friction, and (ii) resistance due to form drag [24]. The resultant pressure distribution over an entire bedform and the flow separation arising from the adverse pressure gradient induce a considerable form drag. In contrast, the skin friction drag oversees the transport of bed sediment particles. Thus, for bedforms, the bed roughness becomes a dynamic parameter being a function of flow characteristics and the bed sediment particles. To capture the effect of form drag, the roughness height is commonly replaced by the composite roughness k_{sc}. Fedele & García [25] reported that the k_{sc} can be approximated as $k_{sc}/d \sim \zeta^{-1/3}$. This relationship is valid for $\zeta < 10^{-3}$ and $D_* < 9.654$, which are common conditions in large alluvial streams with sand ripples and dunes. In the preceding sections, we found that the $\mathcal{F}_{dc} \sim \zeta^{(1+\sigma)/4}$, where it was assumed that the bed roughness height is proportional to the diameter of sediment particles, that is, $k_s \sim d$. However, for bedforms, the k_s is replaced by k_{sc}, yielding $\mathcal{F}_{dc} \sim (k_{sc}/h)^{(1+\sigma)/4} \sim (\zeta k_{sc}/d)^{(1+\sigma)/4}$. Substituting $k_{sc}/d \sim \zeta^{-1/3}$ [25] into this relationship yields $\mathcal{F}_{dc} \sim \zeta^{(1+\sigma)/6}$. This relationship is valid for the alluvial streams with sand ripples and dunes. For $\zeta < 10^{-4}$ (in the enstrophy inertial range), the particle transport is governed by the spectral exponent $\sigma = -3$ and thus, the proposed scaling becomes $\mathcal{F}_{dc} \sim \zeta^{-1/3}$. By contrast, for $10^{-4} < \zeta < 10^{-3}$ (in the energy inertial range), the particle transport is governed by the spectral exponent $\sigma = -5/3$ and thus, the proposed scaling becomes $\mathcal{F}_{dc} \sim \zeta^{-1/9}$.

Downloaded from https://royalsocietypublishing.org/ on 25 October 2022

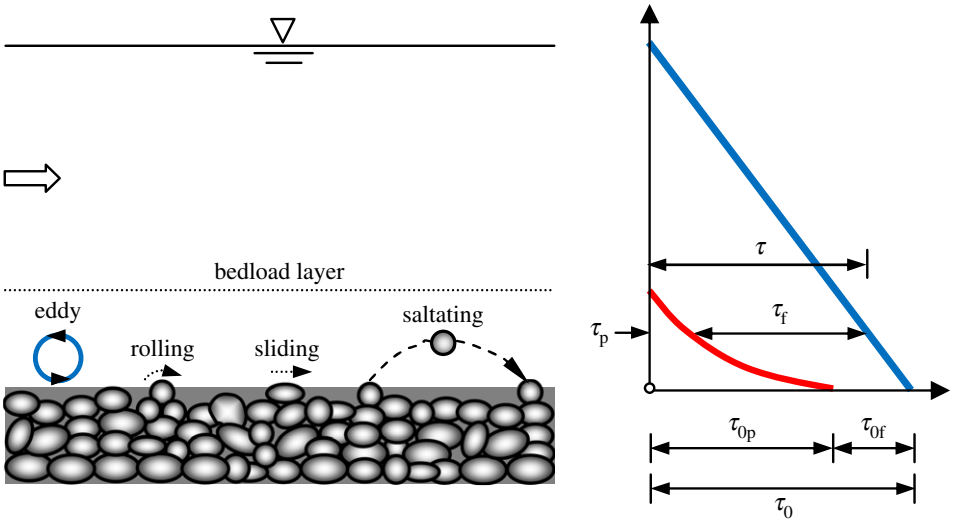

Figure 4. Schematic of bedload transport and the decomposition of applied fluid bed shear stress τ_0 into the dispersive particle shear stress τ_{0p} and the interfacial fluid shear stress τ_{0f}. (Online version in colour.)

4. The scaling law of bedload flux

(a) Theoretical analysis

When the flow velocity exceeds the threshold velocity, the sediment particles are set in motion due to the applied fluid bed shear stress τ_0 in excess of the threshold bed shear stress τ_{0c}. Under such a situation, the transport of sediment particles takes place within a thin layer, called the *bedload layer* (figure 4), in the form of consecutive contacts of the particles with the bed, known as the *bedload transport* [26]. At relatively small excess bed shear stress ($=\tau_0 - \tau_{0c}$), the bedload transport occurs in rolling and/or sliding mode as illustrated in figure 4. On the other hand, with an increase in excess bed shear stress, the sediment particles are transported as a saltating mode, where the particles perform small jumps in the close proximity of the bed, but remain within the bedload layer (figure 4). The bedload flux q_b is usually expressed as the quantity of solid volume of sediment transported per unit time and width. More than a century and a quarter ago, du Boys [27] was the first to provide a mathematical description of the bedload flux stemming from the principle of force balance between the applied fluid force and the frictional resistance. The key feature of the du Boys equation is to relate the bedload flux with the excess bed shear stress. Following the du Boys equation, several investigators attempted to propose the improved version of the bedload flux equations, referred to as the du Boys type equations. A comprehensive compilation of du Boys type equations was done by García [9] and Dey [19]. However, the bedload flux laws proposed by the earlier investigators involve several free exponents, which were determined by the regression analysis of the experimental and/or field data. The state of the art is that an acceptable justification of the appropriate choice of the exponents or the origin of the scaling laws is still lacking.

Let us first attempt to find the scaling law of bedload flux q_b from a simple dimensional analysis. We start with eight plausible variables: q_b, h, d, Δg, ρ_f, ν, τ_0 and τ_{0c}. Thus, in functional form, the equation $f(q_b, h, d, \Delta g, \rho_f, \nu, \tau_0, \tau_{0c}) = 0$ exists. Introducing the bedload transport intensity Φ_b $[=q_b/(\Delta g d^3)^{1/2}]$, the applied Shields parameter Θ $[=\tau_0/(\rho_f \Delta g d)]$, the threshold Shields parameter Θ_c $[=\tau_{0c}/(\rho_f \Delta g d)]$ and the transport stage parameter T_* $[=(\tau_0 - \tau_{0c})/\tau_{0c} = (\Theta - \Theta_c)/\Theta_c]$, and noting that $\Theta_c = G(D_*)$, we obtain the functional relationship as

$$\Phi_b = \phi(T_*, \zeta, D_*). \tag{4.1}$$

Downloaded from https://royalsocietypublishing.org/ on 25 October 2022

We suppose that the motion of sediment particles is confined to the bedload layer, which can be scaled with the diameter of a sediment particle [28]. By definition, the q_b is scaled as $q_b \sim nd^3 v_p$ [19], where n is the number of particles transported per unit area of the sediment bed surface and v_p is the particle velocity. To determine a scaling law of q_b, we require to obtain the scaling laws for n and v_p. Following the conventional mechanics of bedload transport [26], we decompose the applied fluid bed shear stress τ_0 into the dispersive particle shear stress τ_{0p} (that is, the transmitted stress due to momentum exchange for the collision of particles) and the interfacial (or the inter-particle) fluid shear stress τ_{0f} (that is, the transmitted stress due to interfacial fluid), as shown in figure 4. Thus, the formulation is $\tau_0 = \tau_{0p} + \tau_{0f}$. The reason of such a consideration is attributed to the fact that the sediment-laden flow is characterized by the shear which includes the shear between the layers of the particles, and the shear between the particles and the neighbouring fluid. With the removal of a layer of sediment particles by the flow, a dispersive pressure on the subsequent layer of particles is established as a stabilizing force. Bagnold [26] argued that during the bedload transport, the τ_{0f} equals the threshold bed shear stress τ_{0c} for the initiation of particle motion at the bed. Thus, the component τ_{0c} of the applied fluid bed shear stress τ_0 is transferred directly to the immobile-bed particles in the form of a skin frictional stress. On the other hand, the remaining bed shear stress $(\tau_0 - \tau_{0c})$ is directly transferred to the mobile particles in the form of a drag induced bed shear stress τ_{0b}. Thus, we can write $\tau_{0p} \sim \tau_{0b} \sim nf_D$ [29], where f_D is the drag force. The f_D can be scaled with the frictional resistance to flow as $f_D \sim f_R \sim (\rho_p - \rho_f) g d^3$ [19]. Thus, we can write

$$n \sim \frac{\tau_0 - \tau_{0c}}{f_D} \sim \frac{\tau_0 - \tau_{0c}}{(\rho_p - \rho_f) g d^3} \sim \frac{\Theta - \Theta_c}{d^2}. \tag{4.2}$$

The particle dynamics in bedload transport is an intricate phenomenon since the particle dynamics depend on the local fluctuating fluid forces, such as turbulent drag, turbulent lift, collision with neighbouring particles, etc., together with the particle fluctuations and the inter-particle friction. As a consequence, to understand the particle dynamics, proper analysis of the local force system must be pursued [30]. However, to simplify the particle dynamics from the perspective of scaling laws (as main focus of this study), we proceed with the following concept.

Theorem 4.1. *For the bedload flux, the bedload transport intensity obeys the '3/2' and '(1 + σ)/4' scaling laws with the transport stage parameter and the relative roughness, respectively.*

Proof. Since the local bed shear stress is proportional to the square of the local flow velocity, from the relationship $\tau_{0p} = \tau_0 - \tau_{0c}$ [26], at a dynamic equilibrium condition, the particle velocity v_p can be simply obtained as: $v_p^2 \sim v_f^2 - v_{fc}^2$, where v_f is the flow velocity in the immediate vicinity of the sediment bed. Since the v_f is provided by the localized eddy bestriding the fluid–particle interface, the v_f can be scaled as $v_f \sim U$. Subscript 'c' as usual denotes the threshold condition. Hence, it follows:

$$v_p \sim (U^2 - U_c^2)^{1/2} \sim U_c \left(\frac{U^2}{U_c^2} - 1 \right)^{1/2}. \tag{4.3}$$

The particle velocity v_p can be experimentally determined using the particle image velocimetry technique [31–33]. From equation (4.3), we perceive that if $U \approx U_c$, then $v_p \approx 0$, which indicates the threshold condition. Although the experimental observations evidenced the existence of non-zero particle velocity at the threshold, this can be neglected in practical situations [32]. Since $\tau_0 \sim \rho_f U^2$ (applying the friction factor conjecture), we obtain

$$\frac{U}{U_c} = \left(\frac{\tau_0}{\tau_{0c}} \right)^{1/2} = \left(\frac{\Theta}{\Theta_c} \right)^{1/2}. \tag{4.4}$$

Therefore, equation (4.3) reduces to

$$v_p \sim U_c \left(\frac{\Theta}{\Theta_c} - 1 \right)^{1/2}. \tag{4.5}$$

Downloaded from https://royalsocietypublishing.org/ on 25 October 2022

The above scaling law of the particle velocity (see equation (4.5)) is in agreement with the empirical formula of Sekine & Kikkawa [34]. Using equation (3.5), equation (4.5) reduces to

$$v_{\mathrm{p}} \sim (\Delta g d)^{1/2} \zeta^{(1+\sigma)/4} G^{1/2}(D_*) \left(\frac{\Theta}{\Theta_c} - 1 \right)^{1/2}. \tag{4.6}$$

Substituting equations (4.2) and (4.6) into the scaling law $q_{\mathrm{b}} \sim n d^3 v_{\mathrm{p}}$, we finally obtain

$$\Phi_{\mathrm{b}} \sim \frac{(\Theta - \Theta_c)^{3/2}}{\Theta_c^{1/2}} \zeta^{(1+\sigma)/4} G^{1/2}(D_*) \sim T_*^{3/2} \zeta^{(1+\sigma)/4} G^{3/2}(D_*). \tag{4.7}$$

■

(b) Results and discussion

It is revealed that equation (4.7) produces the similar functional form as that obtained from equation (4.1). The '3/2' scaling law with T_* (equation (4.7)) is in conformity with the empirical formulae proposed in earlier studies [28,35–37]. Furthermore, the studies of Damgaard *et al*. [38] evidenced the '3/2' scaling law with T_* for sloping beds ranging from −29° to 30°. They also reported that the bed slope does not influence the '3/2' scaling law for a higher value of Shields parameter. However, for $\sigma = -3$, $-5/3$ and -1, the Φ_{b} obeys the '$-1/2$', '$-1/6$' and '0' scaling law with the relative roughness, respectively.

5. The scaling law of suspended load flux

(a) Theoretical analysis

When the motion of sediment particles in a flowing fluid is such that they are bounded by the surrounding fluid over a longer duration, the sediment particles are said to be in suspension. In a turbulent flow, the mechanism of suspended sediment motion takes place through the transport of sediment particles by the velocity fluctuations and the mixing of sediment particles with the surrounding fluid. For a two-dimensional steady-uniform flow, the complex diffusion process is responsible for the convection of suspended sediment particles. In this case, the motion of suspended sediment particles is hypothesized in a continuum scale as the concentration of sediment transport flux. The transport of the suspended particles occurs convectively when a fluid parcel carrying a certain concentration of sediment particles is transported by the vertical velocity fluctuations to a zone of lower concentration of sediment particles and mixes with the surrounding fluid. Thus, the suspended sediment flux is directly related to the vertical gradient of concentration. Rouse [39] was the first to obtain the vertical distribution of suspended sediment concentration, known as *Rousean distribution*, stemming from the advection–diffusion equation of suspended sediment motion coupled with the Prandtl's mixing length theory. After Rouse [39], several investigators envisioned the mechanism of sediment suspension as a transport of sediment particles governed by the turbulent diffusion and the mixing of fluid. A comprehensive compilation of the studies on suspended sediment concentration was done by Dey [19].

In a two-dimensional steady-uniform flow, the well-known advection–diffusion equation of suspended sediment motion in the vertical direction (that is, the z-direction) reads [19]

$$\varepsilon_{\mathrm{sz}} \partial_z C(z) + w_{\mathrm{s}} C(z) = 0, \tag{5.1}$$

where $\varepsilon_{\mathrm{sz}}$ is the solid diffusivity in the z-direction, $C(z)$ is the local sediment concentration and w_{s} is the terminal fall velocity of sediment particles. The $\varepsilon_{\mathrm{sz}}$ can be related to the turbulent diffusivity $\varepsilon_{\mathrm{tz}}$ as $\varepsilon_{\mathrm{sz}} = \varepsilon_{\mathrm{tz}} \mathcal{S}c^{-1}$, where $\mathcal{S}c$ is the turbulent Schmidt number. The Reynolds shear stress τ_{t} is expressed as $\tau_{\mathrm{t}} = \rho_{\mathrm{f}} \varepsilon_{\mathrm{tz}} s_{\mathrm{l}}$, where s_{l} is the local strain rate in the z-direction [$=u_*/(\kappa z)$] and κ is the von Kármán constant (=0.41). Within the turbulent wall shear layer ($z < 0.2\,h$), the τ_{t} equals the bed shear stress τ_0 ($=\rho_{\mathrm{f}} u_*^2$) yielding $\varepsilon_{\mathrm{tz}} = u_* \kappa z$. The linear variation of $\varepsilon_{\mathrm{tz}}$ with

Downloaded from https://royalsocietypublishing.org/ on 25 October 2022

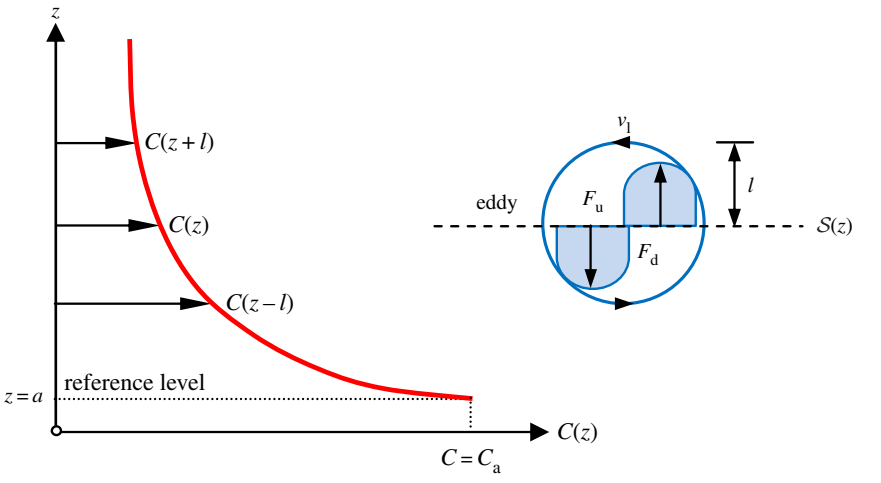

Figure 5. Schematic of the exchange of suspended sediment concentration in turbulent flow. (Online version in colour.)

z is legitimate within the turbulent wall shear layer because the turbulent wall shear layer is realized as the constant stress layer [23]. It is worth emphasizing that the major shortcoming of the Rouse equation is that the equation stems from the linear law of turbulent shear stress in conjunction with the log-law, which is valid under the constant bed shear stress conjecture. It therefore yields a quadratic profile of $\varepsilon_{tz}(z)$ across the boundary layer. On the other hand, the linear relationship of $\varepsilon_{tz}(z)$ can be fairly applied within turbulent wall shear layer because our main intention is concerned with the turbulent wall shear layer, where the dynamics of the suspended load flux is important from the perspective of establishing a suitable scaling law. Thus substituting $\varepsilon_{sz} = \varepsilon_{tz}\mathcal{S}c^{-1}$ and $\varepsilon_{tz} = u_*\kappa z$ into equation (5.1) yields

$$\partial_z C(z) + \mathcal{Z}C(z)z^{-1} = 0, \tag{5.2}$$

where $\mathcal{Z}$ is the *Rouse number* [$=w_s\mathcal{S}c/(\kappa u_*)$].

To integrate equation (5.2), the boundary condition is commonly used as $C(z=a) = C_a$, where a is the reference level and C_a is the reference concentration [39], as shown in figure 5. Thus, integrating equation (5.2) yields

$$C^+ = \left(\frac{z}{a}\right)^{-\mathcal{Z}}, \tag{5.3}$$

where $C^+ = C/C_a$.

Theorem 5.1. *For the suspended load flux, the non-dimensional suspended sediment concentration obeys the '$-\mathcal{Z}$' scaling law with the non-dimensional vertical distance within the wall shear layer.*

Proof. Now, we intend to grasp that how far the '$-\mathcal{Z}$' scaling law (equation (5.3)) can be derived by means of the energetics of turbulent eddies. Let us consider a wetted surface $\mathcal{S}(z)$ at a distance z from the boundary as depicted in figure 5. The local sediment concentration at the wetted surface $\mathcal{S}$ is $C(z)$. The net sediment flux through the wetted surface $\mathcal{S}$ can be obtained by considering the eddies of size l straddling that surface. Since the fluctuations of normal velocity component u_n of an eddy can be scaled with its velocity scale v_l ($u_n \sim v_l$), as discussed earlier, we introduce $u_n = p_1 v_l$, where p_1 is a coefficient being of the order of unity ($p_1 < 1$). The upward sediment flux (volume per unit time and width) is therefore $F_u = (p_1 v_l - w_s)C(z-l)$, while the downward sediment flux is $F_d = (p_1 v_l + w_s)C(z+l)$. Applying the Taylor series expansion, we can fairly approximate $C(z-l) \approx C(z) - l\partial_z C(z)$ and $C(z+l) \approx C(z) + l\partial_z C(z)$. For an equilibrium sediment concentration, the net sediment flux through the wetted surface $\mathcal{S}$ must be zero. Thus,

Downloaded from https://royalsocietypublishing.org/ on 25 October 2022

the equilibrium $F_u = F_d$ yields

$$l v_l p_1 \partial_z C(z) + w_s C = 0. \tag{5.4}$$

The relationship (5.4) represents the governing equation of the particle dynamics of suspended sediment particles governed by the localized turbulent eddy. Since $v_l \sim (\varepsilon l)^{1/3}$, we can write $v_l = p_2(\varepsilon l)^{1/3}$, where p_2 is a coefficient. Using this relationship, equation (5.4) reduces to

$$\varepsilon^{1/3} l^{4/3} p_1 p_2 \partial_z C(z) + w_s C = 0. \tag{5.5}$$

Since the eddies having a size larger than z are unable to completely trigger the wetted surface $\mathcal{S}$ (as evident from figure 5), it can be inferred that the dominant eddies triggering the $\mathcal{S}$ are the eddies of size $l = z$. Now, we pay an attention to the turbulent wall shear layer, where the TKE production rate equals the TKE dissipation rate (since the eddies are in the energy inertial range). Therefore, using the energy balance [23], the Reynolds shear stress can be written as $\tau_t = \rho_f \varepsilon s_l^{-1}$ [23]. Importantly, beyond the turbulent wall shear layer, the energy balance is not legitimate because the individual terms in the TKE budget equation maintain an energy equilibrium. Using $\tau_t = \rho_f u_*^2$ and $s_l = u_*/(\kappa z)$, we obtain $\varepsilon = u_*^3/(\kappa z)$. Substituting this expression of ε into equation (5.5) yields

$$\partial_z C(z) + \frac{\kappa^{4/3}}{p_1 p_2 \mathcal{S}c} \mathcal{Z} C(z) z^{-1} = 0. \tag{5.6}$$

It may be noted that equations (5.2) and (5.6) would be identical if and only if $\kappa^{4/3} = p_1 p_2 \mathcal{S}c$. Since the $\mathcal{S}c$ is of the order of unity, this identity reduces to $\kappa^{4/3} = p_1 p_2$. Substituting $\kappa = 0.41$ and $p_2 = 0.928$ (from Kolmogorov '4/5' scaling law), we obtain $p_1 = 0.33$, which is consistent with the assumption that the p_1 is of the order of unity. Thus, the origin of the '$-\mathcal{Z}$' scaling law is obtained from the perspective of energetics of turbulent eddies. ■

(b) Discussion

The relationship (5.3) can also be written as $\ln C^+ = -\mathcal{Z} \ln z^+ + \mathcal{Z} \ln a^+$, where z^+ is z/h and a^+ is a/h. The a^+ is considered as 0.05 [19]. Figure 6*a* shows the variations of C^+ with z^+ obtained from the '$-\mathcal{Z}$' scaling law within the turbulent wall shear layer ($z^+ < 0.2$) for $\mathcal{Z} = 0.25$, 0.5, 1 and 2. The well-known Rouse equation of concentration, $C^+ = [a^+(1-z^+)/z^+(1-a^+)]^{\mathcal{Z}}$ corresponding to the values of $\mathcal{Z} = 0.25$, 0.5, 1 and 2 is also plotted. From figure 6*a*, it is evident that for $z^+ < 0.2$, the '$-\mathcal{Z}$' scaling law closely corroborates with the Rouse equation, although the scaling law slightly overestimates the Rouse equation. Therefore, the '$-\mathcal{Z}$' scaling law within the turbulent wall shear layer is a substitution for the Rousean $C^+(z^+)$ distribution. Here, it may be interesting to set an inverse problem: for a given Rousean $C^+(z^+)$ distribution, how the Rouse number $\mathcal{Z}$ can be obtained? This problem can be solved by fitting a straight line or drawing a tangent to the given Rousean $C^+(z^+)$ distribution, preferably within the turbulent wall shear layer, where the Rousean $C^+(z^+)$ distribution depicts a constant gradient in the log–log scale (figure 6*a*). Needless to say, the negative value of that constant gradient represents the Rouse number $\mathcal{Z}$, as evident from equation (5.3). Therefore, the Rouse number can be interpreted as the negative gradient of the Rousean $C^+(z^+)$ distribution (in log–log scale) within the turbulent wall shear layer.

The '$-\mathcal{Z}$' scaling law is further compared with some experimental data of Coleman [40] and Lyn [41], as shown in figure 6*b*. Coleman's [40] experimental data for $\mathcal{Z} = 0.75$ and $a^+ = 0.035$ and Lyn's [41] data for $\mathcal{Z} = 1.5$ and $a^+ = 0.072$ are plotted in figure 6*b*. It shows that the '$-\mathcal{Z}$' scaling law has an excellent agreement with the experimental data within the turbulent wall shear layer ($z^+ < 0.2$).

Downloaded from https://royalsocietypublishing.org/ on 25 October 2022

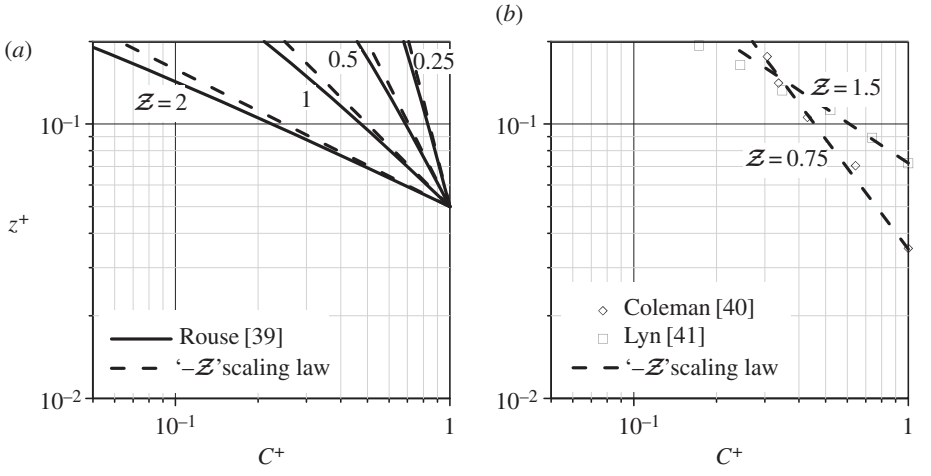

Figure 6. Non-dimensional concentration C^+ as a function of z^+ for (*a*) different values of $\mathcal{Z}$ and (*b*) $\mathcal{Z} = 0.75$ and 1.5 and the experimental data of Coleman [40] and Lyn [41].

6. The scaling law of scour in a contracted stream

(a) Theoretical analysis

Scour in a contracted stream (for example, scour within a channel contraction) is one of the common problems of sediment transport. Contractions of channel width to construct bridges, weirs, and other hydraulic structures are practical examples for the cases of contracted streams. Owing to the concentration of streamlines in a contraction, the flow is convectively accelerated in the contracted portion resulting in a higher flow velocity and in turn, an enhanced bed shear stress that can erode the sediment bed in the contracted portion. Figure 7*a*,*b* shows a schematic view of scour within a channel contraction for a rectangular channel. The approach channel width and the approach flow depth are B_1 and h_1, respectively, while the contracted channel width and the contracted flow depth are B_2 and h_2, respectively. When the approach flow enters into the contracted portion, the flow concentration in the contracted portion is enhanced as described in figure 7*a*. As a result of which, the sediment bed is eroded due to an increased velocity within the contraction as shown in figure 7*b*. Thus, the scour hole within the contraction is developed. The size of the scour hole grows with time causing a gradual reduction of flow velocity within the contraction in accordance with the increase in flow area with the development of scour hole (figure 7*b*). Eventually, an equilibrium scour is attained when the flow velocity in the contracted portion reduces to a threshold velocity and is unable to dislodge the sediment particles from the scour hole.

We are now going to find the scaling law of the equilibrium scour depth d_s from the dimensional analysis. Let us denote the sum of the equilibrium scour depth d_s and the approach flow depth h_1 as D $(=d_s + h_1)$. We start with nine plausible variables: D, U_1, B_1, B_2, h_1, d, Δg, ρ_f and ν. Thus, in functional form, the equation $f(D, U_1, B_1, B_2, h_1, d, \Delta g, \rho_f, \nu) = 0$ exists. Denoting the densimetric Froude number for the approach flow $\mathcal{F}_{d1}$ $[=U_1/(\Delta g d^3)^{1/2}]$, the relative roughness ζ_1 (ratio of particle diameter d to approach flow depth h_1) and the channel contraction ratio r $(=B_2/B_1)$, we obtain following functional form:

$$\frac{D}{h_1} = \phi(\mathcal{F}_{d1}, r, \zeta_1, D_*). \tag{6.1}$$

Theorem 6.1. *For the scour in contracted streams, the non-dimensional scour depth obeys the '$4/(3-\sigma)$', '$-4/(3-\sigma)$' and '$-(1+\sigma)/(3-\sigma)$' scaling laws with the densimetric Froude number, the channel contraction ratio and the relative roughness, respectively.*

Downloaded from https://royalsocietypublishing.org/ on 25 October 2022

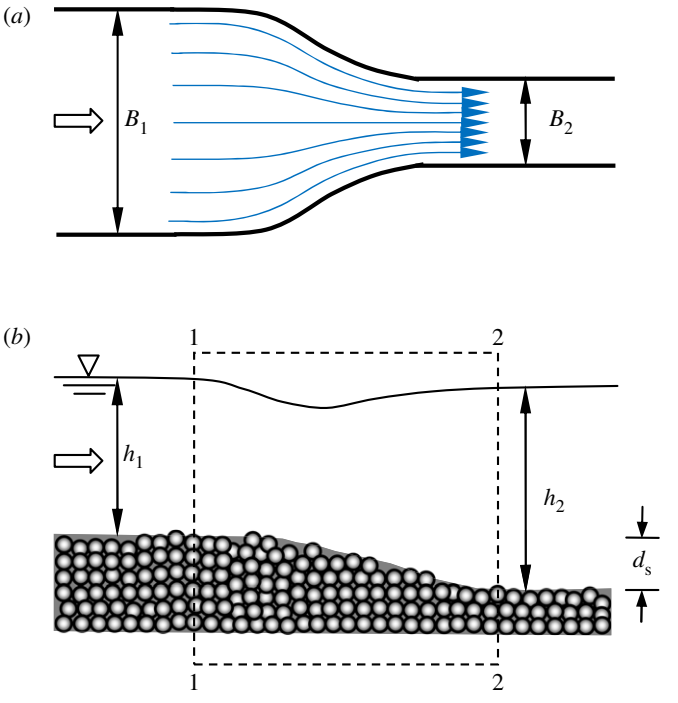

Figure 7. Schematic of scour in a contracted stream: (*a*) plan view and (*b*) elevation view. The approach channel width and the approach flow depth are B_1 and h_1, respectively. The contracted channel width and the contracted flow depth are B_2 and h_2, respectively. The equilibrium scour depth is d_s. (Online version in colour.)

Proof. The continuity equation of fluid flow satisfies

$$U_1 h_1 B_1 = U_2|_{U_2=U_c} h_2 B_2. \tag{6.2}$$

Neglecting the difference in velocity heads and the loss through the transition, the energy per unit weight of the fluid between the approach section and the contracted section yields $d_s = h_2 - h_1$. With this and using equation (6.2), we obtain

$$\frac{D}{h_1} = \frac{d_s + h_1}{h_1} = \frac{U_1}{U_2|_{U_2=U_c}} \frac{1}{r}. \tag{6.3}$$

From equation (3.5), the threshold velocity in the contracted channel is given by

$$U_2|_{U_2=U_c} \sim (\Delta g d)^{1/2} \left(\frac{d}{h_2}\right)^{(1+\sigma)/4} G^{1/2}(D_*) \sim (\Delta g d)^{1/2} \left(\frac{D}{h_1}\right)^{-(1+\sigma)/4} \zeta_1^{(1+\sigma)/4} G^{1/2}(D_*). \tag{6.4}$$

Substituting equation (6.4) into equation (6.3) yields

$$\frac{D}{h_1} \sim \mathcal{F}_{d1}^{4/(3-\sigma)} r^{-4/(3-\sigma)} \zeta_1^{-(1+\sigma)/(3-\sigma)} G^{-2/(3-\sigma)}(D_*). \tag{6.5}$$

■

(b) Results and discussion

For $\sigma = -3, -5/3$ and -1, equation (6.5) yields $D/h_1 \sim \mathcal{F}_{d1}^{2/3} r^{-2/3} \zeta_1^{1/3}$, $\mathcal{F}_{d1}^{6/7} r^{-6/7} \zeta_1^{1/7}$ and $\mathcal{F}_{d1} r^{-1} \zeta_1^0$, respectively. Now we intend to validate the proposed scaling laws with the experimental data. Since the spectral exponent $\sigma = -3$ signifies the limit of the hydraulically smooth flow, the roughness elements become of the order of viscous sublayer thickness. As a result, the experimental data can hardly be obtained for this case. This is because of the fact that most of the

Downloaded from https://royalsocietypublishing.org/ on 25 October 2022

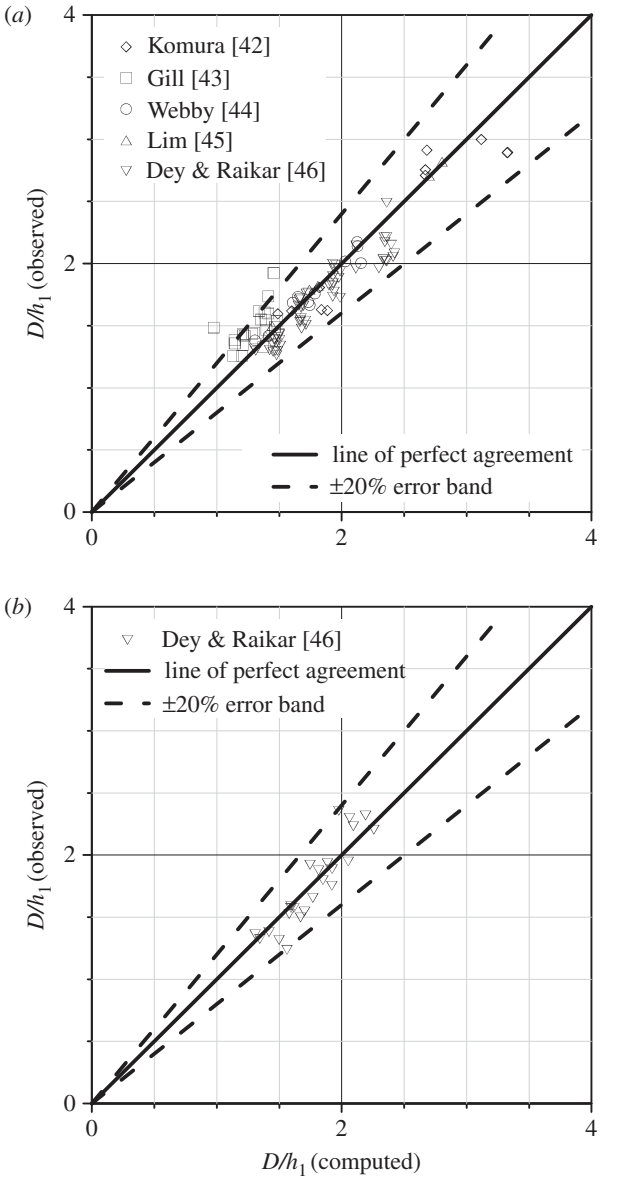

Figure 8. Comparison of the scaling laws of D/h_1 for (*a*) $\sigma = -5/3$ with the experimental data in earlier studies [42–46] and (*b*) $\sigma = -1$ with the experimental data of Dey & Raikar [46].

laboratory and field experimental data related to scour problems are subjected to hydraulically transitional and/or rough flow regimes. Therefore, we only validate the proposed scaling laws for $\sigma = -5/3$ and -1 with the experimental data. Figure 8*a* shows the comparison of the proposed scaling law of D/h_1 for $\sigma = -5/3$ with the experimental data in earlier studies [42–46]. These experimental data include sand and gravel with the relative roughness in the range of $10^{-4} < \zeta_1 < 10^{-1}$, which properly satisfies the validity of the spectral exponent $\sigma = -5/3$. The ±20% error band is also depicted for a quantitative understanding of the experimental data scatter (due to the variability of $G(D_*)$ in transitional-rough flow) from the best-fitted straight line. Figure 8*a*, however, shows an excellent matching of the proposed scaling law with the experimental data. On the other hand, figure 8*b* shows the comparison of the proposed scaling law of D/h_1 for $\sigma = -1$ with the experimental data of Dey & Raikar [46]. These experimental data

Downloaded from https://royalsocietypublishing.org/ on 25 October 2022

include large gravel (macro-roughness) with the relative roughness in the range of $10^{-1} < \zeta_1 < 1$, which fairly satisfies the validity of the spectral exponent $\sigma = -1$. The ±20% error band is also shown for an understanding of experimental data scatter. In this case, the agreement of the proposed scaling law of D/h_1 for $\sigma = -1$ with the experimental data is satisfactory.

We are also interested to validate the proposed scaling laws of D/h_1 with the empirical formulae reported by previous investigators. The empirical formula of Straub [47] shows that the D/h_1 is scaled with $r^{-6/7}$, which is in agreement with the present study for the spectral exponent $\sigma = -5/3$. Moreover, the proposed scaling law of D/h_1 for $\sigma = -5/3$ completely corresponds to the formulae of Gill [43] and Laursen [48]. Both Gill [43] and Laursen [48] reported the formula as $D/h_1 = 0.424\mathcal{F}_{d1}^{6/7} r^{-6/7} \zeta_1^{1/7}$. According to the empirical formula of Lim [45], the scaling of D/h_1 follows $D/h_1 \sim \mathcal{F}_{d1}^{3/4} r^{-3/4} \zeta_1^{1/4}$, which is somewhat different from the proposed scaling laws. It is important to note that since the empirical formulae are developed by the regression fittings of the experimental and/or field data, which may contain uncertainties, the free exponents involved in the empirical formulae can differ significantly depending on the availability and the quality of raw experimental and field data. However, the empirical formulae of Gill [43] and Laursen [48] completely corroborate with the proposed scaling law in the energy inertial range ($\sigma = -5/3$). By contrast, the empirical formula of Lim [45], in general, tends to correspond to the proposed scaling law of D/h_1 for $\sigma = -5/3$.

7. Conclusion

The origin of the scaling laws of sediment transport under turbulent flow is investigated from the perspective of the phenomenological theory of turbulence. The link between the scaling laws of sediment transport and the laws of turbulent energy spectrum is explored from the concepts of the energy cascade (energy inverse cascade for two-dimensional turbulence and energy forward cascade for three-dimensional turbulence), the enstrophy cascade and the '−1' spectral law of wall-bounded turbulence. This study shows that the origin of the scaling laws of sediment transport can be explained by applying the fundamental laws of turbulent energy spectrum (for both two- and three-dimensional turbulence), where the energy cascade, the enstrophy cascade and the '−1' spectral law play a significant role for the momentum transfer of turbulent eddies. This study analyses the scaling laws of four fundamental problems of sediment transport: the incipient motion of sediment particles, the bedload flux, the suspended load flux and the scour in a contracted stream. It is revealed that the phenomenological theory provides a shorthand approach to find the origin of the scaling laws. This study also provides a physical insight into the sediment transport problems by elucidating the interaction between the localized turbulence and the sediment particles. The proposed concept can be further used to analyse many other practical problems, which involve the fluid–sediment interaction.

Data accessibility. All the data of this study can be obtained from the authors.
Authors' contributions. The authors of this paper contributed jointly.
Competing interests. We declare we have no competing interests.
Funding. No funding has been received for this article.

References

1. Kolmogorov AN. 1941 The local structure of turbulence in incompressible viscous fluids at very large Reynolds numbers. *Dokl. Akad. Nauk SSSR* **30**, 299–303.
2. Frisch U. 1995 *Turbulence: the legacy of A. N. Kolmogorov*. Cambridge, UK: Cambridge University Press.
3. Sreenivasan KR, Antonia RA. 1997 The phenomenology of small-scale turbulence. *Annu. Rev. Fluid Mech.* **29**, 435–472. (doi:10.1146/annurev.fluid.29.1.435)
4. Nikora V. 1999 Origin of the '−1' spectral law in wall-bounded turbulence. *Phys. Rev. Lett.* **83**, 734–736. (doi:10.1103/PhysRevLett.83.734)

Downloaded from https://royalsocietypublishing.org/ on 25 October 2022

5. Gioia G, Bombardelli FA. 2002 Scaling and similarity in rough channel flows. *Phys. Rev. Lett.* **88**, 014501. (doi:10.1103/PhysRevLett.88.014501)
6. Kraichnan RH. 1967 Inertial ranges in two-dimensional turbulence. *Phys. Fluids* **10**, 1417–1423. (doi:10.1063/1.1762301)
7. Rutgers MA. 1998 Forced 2D turbulence: experimental evidence of simultaneous inverse energy and forward enstrophy cascades. *Phys. Rev. Lett.* **88**, 2244–2247. (doi:10.1103/PhysRevLett.81.2244)
8. Gioia G, Chakraborty P. 2006 Turbulent friction in rough pipes and the energy spectrum of the phenomenological theory. *Phys. Rev. Lett.* **96**, 044502. (doi:10.1103/PhysRevLett.96.044502)
9. García MH. 2008 *Sedimentation engineering: processes, measurements, modeling, and practice*. Reston, VA: American Society of Civil Engineers.
10. Shields AF. 1936 Anwendung der Ahnlichkeitsmechanik und der Turbulentzforschung auf die Geshiebebewegung, Mitt. Preuss. Versuchsanst. Wasserbau Schiffbau, vol. 26, 26 pp. (English translation by W. P. Ott & J. C. van Uchelen, 1936. *Rep. 167*, 36 pp., Calif. Inst. of Technol., Pasadena).
11. Ali SZ, Dey S. 2016 Hydrodynamics of sediment threshold. *Phys. Fluids* **28**, 1–22. (doi:10.1063/1.4955103)
12. Lischtvan LL, Lebediev VV. 1959 Gidrologia i Gidraulika v Mostovom Doroshnom, Straitielvie. Leningrad (Hydrology and Hydraulics in Bridge and Road Building), Gidrometeoizdat, Leningrad.
13. Neill CR. 1967 Mean velocity criterion for scour of course uniform bed material. In *Proc. of the 12th Congress of Int. Association for Hydraulic Research, Fort Collins, Colorado, USA*, vol. 3, pp. 46–54. Madrid, Spain: IAHR.
14. Ashida K, Bayazit M. 1973 Initiation of motion and roughness of flows in steep channels. In *Proc. of the 15th Congress of Int. Association for Hydraulic Research, Istanbul, Turkey*, vol. 1, pp. 475–484. Madrid, Spain: IAHR.
15. Olivero ML. 1984 *Movimiento incipiente de partículas en flujo torrencial.* Application Report for Associate Professor, University de Los Andes, Mérida, Venezuela, pp. 169.
16. Aguirre-Pe J, Fuentes R. 1991 Movement of big particles in steep, macro-rough streams. In *Proc. of the 24th Congress of Int. Association for Hydraulic Research, Madrid, Spain*, pp. 149–158. Madrid, Spain: IAHR.
17. Bathurst JC, Graf WH, Cao HH. 1983 Initiation of sediment transport in steep channels with coarse bed material. In *Mechanics of sediment transport* (eds BM Summer, A Müller), pp. 207–213. Rotterdam, The Netherlands: ASCE Press.
18. Bathurst JC, Cao HH, Graf WH. 1984 *The data from the EPFL study of hydraulics and sediment transport in a steep flume*. Report no. CH-1015. Ecole Polytechnique Fédérale de Lausanne, Lausanne, Switzerland, 64.
19. Dey S. 2014 *Fluvial hydrodynamics: hydrodynamic and sediment transport phenomena*. Berlin, Germany: Springer.
20. Vassilicos JC. 2015 Dissipation in turbulent flows. *Annu. Rev. Fluid Mech.* **47**, 95–114. (doi:10.1146/annurev-fluid-010814-014637)
21. Ferraro D, Servidio S, Carbone V, Dey S, Gaudio R. 2016 Turbulence laws in natural bed flows. *J. Fluid Mech.* **798**, 540–571. (doi:10.1017/jfm.2016.334)
22. Saddoughi SG, Veeravalli SV. 1994 Local isotropy in turbulent boundary layers at high Reynolds number. *J. Fluid Mech.* **268**, 333–372. (doi:10.1017/S0022112094001370)
23. Pope SB. 2000 *Turbulent flows*. Cambridge, UK: Cambridge University Press.
24. Coleman SE, Nikora VI, Mclean SR, Clunie TM, Schlicke T, Melville BW. 2006 Equilibrium hydrodynamics concept for developing dunes. *Phys. Fluids* **18**, 1–12. (doi:10.1063/1.2358332)
25. Fedele JJ, García MH. 2001 Hydraulic roughness in alluvial streams: a boundary layer approach. In *Riverine, coastal and estuarine morphodynamics* (eds G Seminara, P Blondeaux), pp. 37–60. Berlin, Germany: Springer.
26. Bagnold RA. 1956 The flow of cohesionless grains in fluids. *Phil. Trans. R. Soc. Lond. A* **249**, 235–297. (doi:10.1098/rsta.1956.0020)
27. du Boys MP. 1879 Le rhone et les rivieres a lit affouillable. *Ann. Ponts chaussés* **18**, 141–195.
28. Einstein HA. 1950 The bed-load function for sediment transportation in open channel flows. Technical bulletin 1026, United States Department of Agriculture, Soil Conservation Service, Washington DC.
29. Engelund F, Fredsøe J. 1976 A sediment transport model for straight alluvial channels. *Nord. Hydrol.* **7**, 293–306.

Downloaded from https://royalsocietypublishing.org/ on 25 October 2022

30. van Rijn LC. 1984 Sediment transport, part I: bed load transport. *J. Hydraul. Eng.* **110**, 1431–1456. (doi:10.1061/(ASCE)0733-9429(1984)110:10(1431))
31. Radice A, Malavasi S, Ballio F. 2006 Solid transport measurements through image processing. *Exp. Fluids* **41**, 721–734. (doi:10.1007/s00348-006-0195-9)
32. Lajeunesse E, Malverti L, Charru F. 2010 Bed load transport in turbulent flow at the grain scale: experiments and modelling. *J. Geophys. Res.* **115**, 1–16. (doi:10.1029/2009JF001628)
33. Roseberry JC, Schmeeckle MW, Furbish DJ. 2012 A probabilistic description of the bed load sediment flux: 2. Particle activity and motions. *J. Geophys. Res.* **117**, 1–21. (doi:10.1029/2012JF002353)
34. Sekine M, Kikkawa H. 1992 Mechanics of saltating grains. II. *J. Hydraul. Eng.* **118**, 536–558. (doi:10.1061/(ASCE)0733-9429(1992)118:4(536))
35. Meyer-Peter E, Müller R. 1948 Formulas for bed-load transport. In *Proc. of the 2nd Meeting of Int. Association for Hydraulic Research, Stockholm, Sweden*, vol. 3, pp. 39–64. Madrid, Spain: IAHR.
36. Fernandez Luque R, van Beek R. 1976 Erosion and transport of bed-load sediment. *J. Hydraul. Res.* **14**, 127–144. (doi:10.1080/00221687609499677)
37. van Rijn LC. 1984 Sediment pick-up functions. *J. Hydraul. Eng.* **110**, 1494–1502. (doi:10.1061/(ASCE)0733-9429(1984)110:10(1494))
38. Damgaard JS, Whitehouse RJS, Soulsby RL. 1997 Bed-load sediment transport on steep longitudinal slopes. *J. Hydraul. Eng.* **123**, 1130–1138. (doi:10.1061/(ASCE)0733-9429(1997)123:12(1130))
39. Rouse H. 1937 Modern conceptions of the mechanics of turbulence. *Trans. Am. Soc. Civ. Eng.* **102**, 463–505.
40. Coleman NL. 1986 Effects of suspended sediment on the open-channel velocity distribution. *Water Resour. Res.* **22**, 1377–1384. (doi:10.1029/WR022i010p01377)
41. Lyn DA. 1986 Turbulence and turbulent transport in sediment-laden open-channel flows. PhD thesis, California Institute of Technology, California, USA.
42. Komura S. 1966 Equilibrium depth of scour in long constrictions. *J. Hydraul. Div.* **92**, 17–37.
43. Gill MA. 1981 Bed erosion in rectangular long constriction. *J. Hydraul. Div.* **107**, 273–284.
44. Webby MG. 1984 General scour at contraction. RRU bulletin 73, National Roads Board, Bridge Design and Research Seminar, New Zealand, pp. 109–118.
45. Lim SY. 1993 Clear water scour in long contractions. *Proc. Inst. Civ. Engrs Wat. Marit. Energy* **101**, 93–98. (doi:10.1680/iwtme.1993.23590)
46. Dey S, Raikar RV. 2005 Scour in long contractions. *J. Hydraul. Eng.* **131**, 1036–1049. (doi:10.1061/(ASCE)0733-9429(2005)131:12(1036))
47. Straub LG. 1934 Effect of channel contraction works upon regimen of movable bed streams. *Trans. Am. Geophys. Union* **15**, 454–463. (doi:10.1029/TR015i002p00454)
48. Laursen EM. 1963 An analysis of relief bridge scour. *J. Hydraul. Div.* **89**, 93–118.